Cerebral Cortex December 2013;23:3007–3015
doi:10.1093/cercor/bhs292
Advance Access publication September 17, 2012

Quantification and Discrimination of Abnormal Sulcal Patterns in Polymicrogyria

Kiho Im[1,2], Rudolph Pienaar[2,3], Michael J. Paldino[3], Nadine Gaab[4], Albert M. Galaburda[5] and P. Ellen Grant[1,2,3]

[1]Division of Newborn Medicine, [2]Center for Fetal Neonatal Neuroimaging and Developmental Science, [3]Department of Radiology, [4]Laboratories of Cognitive Neuroscience, Division of Developmental Medicine, Boston Children's Hospital, Harvard Medical School, and [5]Division of Behavioral Neurology, Department of Neurology, Beth Israel Deaconess Medical Center, Boston, MA , USA

Address correspondence to Kiho Im, Boston Children's Hospital, 300 Longwood Avenue, Boston, MA 02115, USA. Email: kiho.im@childrens.harvard.edu

Polymicrogyria (PMG) is a malformation of cortical development characterized by an irregular gyral pattern and its diagnosis and severity have been qualitatively judged by visual inspection of imaging features. We aimed to provide a quantitative description of abnormal sulcal patterns for individual PMG brains using our sulcal graph-based analysis and examined the association with language impairment. The sulcal graphs were constructed from magnetic resonance images in 26 typical developing and 18 PMG subjects and the similarity between sulcal graphs was computed by using their geometric and topological features. The similarities between typical and PMG groups were significantly lower than the similarities measured within the typical group. Furthermore, more lobar regions were determined to be abnormal in most patients when compared with the visual diagnosis of PMG involvement, suggesting that PMG may have more global effects on cortical folding than previously expected. Among the PMG, the group with intact language development showed sulcal patterns more closely matched with the typical than the impaired group in the left parietal lobe. Our approach shows the potential to provide a quantitative means for detecting the severity and extent of involvement of cortical malformation and a greater understanding of genotype–phenotype and clinical-imaging features correlations.

Keywords: cortical malformation, graph matching, polymicrogyria, sulcal pattern

Introduction

Polymicrogyria (PMG) is a malformation of cortical development in which the process of normal cortical development is interrupted during the late stages of neuronal migration; the result is the formation of multiple small gyri and abnormal cortical lamination (Barkovich 2010). Patterns of cortical involvement have been classified and described according to the distribution of the PMG including bilateral frontal (Guerrini et al. 2000), bilateral frontoparietal (Piao et al. 2002; Chang et al. 2003), bilateral perisylvian (Kuzniecky et al. 1993), bilateral parieto-occipital (Guerrini et al. 1997), generalized PMG (Chang et al. 2004), and also unilateral PMG (Chang et al. 2006). A recent study determined the relative frequencies of different PMG patterns with 328 patients and defined the spectrum of their imaging features (Leventer et al. 2010). The main patterns of PMG were perisylvian (61%), generalized (13%), frontal (5%), and parasagittal parieto-occipital (3%) and each of the patterns was further divided into subtypes based on distinguishing imaging characteristics (Leventer et al. 2010).

This interest in subtype distinction arises from the desire to better understand the etiology and clinical consequences of the PMG. For example, different topographic distributions of PMG involvement can be caused by mutations in different genes involved in regional patterning of the cerebral cortex at early stages of development (Rakic 2004; Jansen and Andermann 2005). In particular, it was found that bilateral frontoparietal PMG was associated with mutations of the *GPR56* gene (Piao et al. 2004). In addition, the clinical presentation appears to be related to the extent of cortical involvement of PMG with patients showing more extensive regions of PMG were more likely to present with a global developmental delay and at an earlier age than those showing more focal involvement (Barkovich and Kjos 1992; Barkovich 2010; Leventer et al. 2010). However, to date, the diagnosis and classification of PMG patterns have been qualitatively assessed by a visual inspection of 2D images by a neuroradiologist. As a result subtle regions of PMG may be missed, the extent of lobar involvement variably reported and there is the potential for inter-reader variability. In addition visual assessment of the type and extent of PMG cannot provide a truly quantitative evaluation. An accurate quantitative characterization of abnormal sulcal patterns in PMG could help optimize and standardize characterization of PMG as well as provide a basis for more detailed genotype–phenotype correlation and clinical phenotype-imaging correlation.

Our recent study suggested a method for performing a comprehensive and quantitative analysis of sulcal patterns using sulcal pits (Im, Pienaar et al. 2011). Sulcal pits are defined as the deepest local points of sulci and their spatial distribution is hypothesized to be related to brain functions that are under tight genetic control (Regis et al. 2005; Lohmann et al. 2008; Im et al. 2010; Mangin et al. 2010). We represented the sulcal pattern as a graph structure with sulcal pits as nodes and automatically compared different sulcal graphs by computing a similarity value. Our method considers not only the geometric features of sulcal folds themselves, but also intersulcal geometric and topological relationships to highlight the interrelated arrangement and patterning of sulcal folds (Im, Pienaar et al. 2011). PMG brains show irregular gyral patterns with abnormally oriented multiple small gyri. We hypothesized that their sulcal pits and sulcal segments would show different positions, depth, size, and spatial arrangements compared with normal and could effectively characterize individual cortical involvement in PMG.

In this study, we quantified abnormal sulcal patterns in PMG brains using the graph-based sulcal pattern analysis at the lobar regional level to provide a more explicit and detailed description of their anatomical phenotype. To determine whether there was a relationship between our lobar regional quantitative measurement and a clinical feature, we examined the association with language impairment (deficits in comprehension, production, and use of language), which

is one of the typical features of developmental delay in PMG (Guerreiro et al. 2002; Piao et al. 2004; Jansen and Andermann 2005; Saporta et al. 2011). Because PMG patterns are highly heterogeneous in terms of topographic distribution, in addition to the group analysis, we compared the quantitative characterization with two neuroradiologist's visual diagnosis of lobar involvement for individual PMG subjects. To evaluate the sensitivity of our methodology, we analyzed an additional feature, cortical curvature, which has been widely used to quantify the shape of the cortical folds (Gaser et al. 2006; Rettmann et al. 2006; Im, Lee, Lyttelton et al. 2008; Im, Lee, Seo et al. 2008; Pienaar et al. 2008; Mangin et al. 2010), and compared it with our approach.

Materials and Methods

Participants

PMG patients were identified retrospectively from a search of existing patient data at the Boston Children's Hospital in the United States of America. Inclusion in this study was based on the following criteria: 1) pediatric age group (younger than or equal to 18 years), 2) confirmed clinical diagnosis of epilepsy, based on a history of at least two separable seizure events, 3) diagnosis of PMG established by pathology or magnetic resonance imaging (MRI), 4) MRI examination performed at 3 T, 5) language development characterized by a pediatric neurologist. Refinements to the above-defined patient population were based on the inspection of significant motion or other artifactual degradation of image quality.

An age-matched typical developing control group was also retrospectively identified from existing patient data with the following inclusion criteria: 1) subjects presented for evaluation of headache, 2) subjects must have had an MRI examination of the brain performed at 3 T (identical protocol to the exam performed in the patient group), 3) subjects must have had their language development characterized as typical by a pediatric neurologist. Exclusion criteria for the normative cohort were as follows: 1) any neurologic abnormality by history or physical exam, 2) any degree of language impairment, 3) any MRI abnormality.

The final sample of this study consisted of 26 typical controls (n [male/female]: 8/18, age [mean ± SD, range]: 8.9 ± 5.0, 2–18 years) and 18 PMG patients (n = 12/6, age: 8.8 ± 5.3, 2–18 years). This study was approved by the local Institutional Review Board.

MRI Acquisition and Diagnosis

All imaging was performed on two 3 T magnets (Siemens, Tim Trio). The following sequence was obtained for each patient: Sagittal Magnetization Prepared Rapid Gradient Echo (MPRAGE; TR/TE: 2530 ms/3.39 ms; 1 acquisition; flip angle: 7 degrees, inversion time: 1100 ms; FOV: 22 cm; acceleration factor: 2; voxel size [mm]: 1 × 1 × 1).

Based on standard anatomic images, the location of the dysplastic cortex in PMG patients was evaluated by two pediatric neuroradiologists blinded to the sulcal patterning analysis and language data. Specifically, each lobe in each hemisphere of each patient was categorized as involved or not-involved by PMG by visual inspection (Fig. 1). The 18 patients were divided into three groups based on their language development: 1) intact: appropriate for age [n = 8], 2) mild-to-moderate impairment: some language development, but delayed by comparison with piers (either expressive or receptive) [n = 6], 3) profound impairment: the absence of oral language [n = 4]. Table 1 presents clinical notes of the regional and hemispherical PMG involvement and language development assessment observed in our experimental cohort.

Image Processing

The images were processed to extract cortical surfaces using the FreeSurfer pipeline (Dale et al. 1999; Fischl et al. 1999). This processing includes removal of non-brain tissue (Segonne et al. 2004), Talairach transformation, tissue segmentation, intensity normalization (Sled et al. 1998), tessellation of the gray matter white matter boundary, automated topology correction (Fischl et al. 2001; Segonne et al. 2007), and surface deformation following intensity gradients to optimally place the gray/white matter and gray matter/cerebrospinal fluid boundaries (Dale et al. 1999). Once the cortical models were reconstructed, they were automatically parcellated into anatomical regions based on lobar and gyral/sulcal structure (Fischl et al. 2004; Desikan et al. 2006). We used the left and right whole hemispheres and lobar

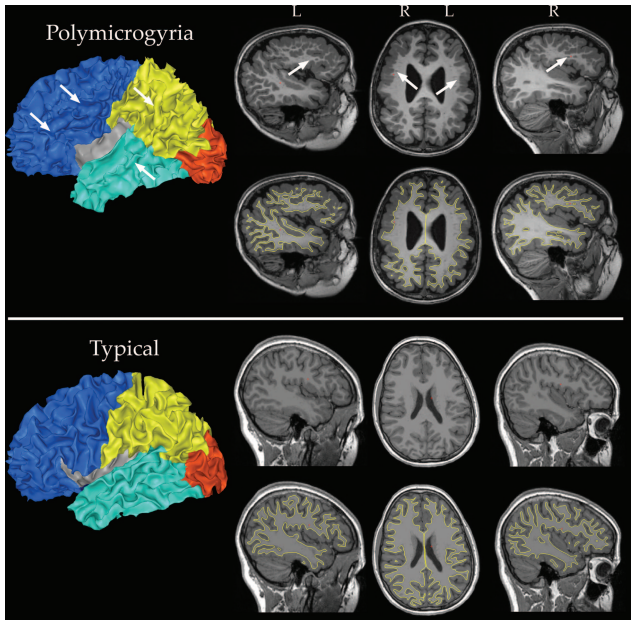

Figure 1. Visual diagnosis of PMG involvement and the reconstruction of the white matter surface and its lobe parcellation from individual PMG MRI data (L: left, R: right). The white matter surface is overlapped to a raw volume image. High frequency gyration is represented with abnormal shape in the reconstructed surface. Sagittal and axial images and the surface model demonstrate dysplastic cortex involving the frontal lobes and perisylvian regions of the temporal and parietal lobes (arrows). It can be compared with the white matter surface and volume images of an individual typical subject.

Table 1

Clinical data (age, gender, PMG regional involvement, and language score) for individual PMG patients

Age (year)	Gender	Lobar regional involvement of PMG	Language score
17	M	R-F	1
14	M	R-T, R-P, R-O	2
16	M	B-F, B-P	2
9	F	B-F, R-T, R-P, R-O	1
9	M	L-F, L-T, L-P	1
6	M	B-F, B-T, B-P	2
6	F	R-F, R-T, R-P	1
6	F	L-F, L-T, L-P	1
4	F	B-F	2
18	M	B-T, B-O	1
5	M	L-F, L-P	2
3	M	B-F, B-T	3
3	F	B-F, B-T, R-P	3
2	M	B-F, B-T, B-P	3
8	F	L-F, L-T, L-P	2
14	M	L-F, L-T, L-P	1
5	M	B-F, B-T, B-P	3
14	M	R-F	1

M, Male; F, Female; B, both hemispheres; L, left hemisphere; R, right hemisphere; F, frontal; T, temporal; P, parietal; O, occipital.

Language score data: 1, intact; 2, mild-to-moderate impairment; 3, profound impairment.

regions (including inter-hemispheric and basal surfaces) of the white matter surface (gray/white matter boundary) for sulcal pattern analysis in this study. The reconstruction of the white matter surface from individual PMG MRI data and its lobe parcellation were visually inspected for each subject to ensure accuracy. An example PMG subject and typical white matter surface are shown in Figure 1. The high frequency of small gyri in PMG was represented as abnormal shape in the reconstructed surface. The same surface reconstruction method was used for the cortical thickness analysis of patients with PMG in a previous study (Oliveira et al. 2009).

Quantitative Comparison of Sulcal Pattern Using Sulcal Graph Matching

The sulcal pattern was represented with a graph structure using sulcal pits as the nodes. Sulcal pits are defined as the deepest local point in a sulcal catchment basin. Sulcal pits and their sulcal catchment basins can be automatically identified by using a sulcal depth map on the white matter surface (Im et al. 2010). The sulcal depth was computed by integrating the dot product of the movement vector during inflation with the surface normal vector at each vertex (Fischl et al. 1999). We used a watershed segmentation algorithm based on a depth map to extract sulcal pits on triangular meshes (Im et al. 2010) (Fig. 2). Each sulcal pit corresponded to a node in the graphical representation. If sulcal basins met, sulcal pits in those basins were connected with an undirected edge (Fig. 2). To quantitatively compare different sulcal graph sets, we used the geometric features of nodes (3D position [x, y, z], depth [d] and the area of sulcal basin [s]) and their relationship. We also exploited the features of graph topology (the number of edges and the paths between nodes [c]) to reflect the interrelated sulcal arrangement and patterning. These features were weighted to give their relative importance, $F = (w_x x, w_y y, w_z z, w_d d, w_s s, w_c c)$. We determined the optimal match having the minimum difference of the features between two sulcal graphs and then computed their similarity, which ranged from 0 to 1, by using a spectral matching technique (Leordeanu and Hebert 2005; Lyu et al. 2010; Im, Pienaar et al. 2011). A pair of graphs, P and Q, containing m and n nodes, respectively, can be represented as follows:

$$P = \{p_1, p_2, \ldots, p_m\} \text{ and } Q = \{q_1, q_2, \ldots, q_n\}.$$

We constructed a matrix M by measuring affinity values, $F(p_i) - F(q_j)$, of all possible pairs of two nodes in graphs P and Q. The relationships of the nodes within the same graph were compared between P and Q, $(F(p_i) - F(p_k)) - (F(q_j) - F(q_l))$, which also composed the affinity matrix M. Next, the M was used to choose a subset matrix C of consistent pairs, determining the optimal match between P and Q, and their similarity was defined as the mean of affinity values from C (Leordeanu and Hebert 2005; Im, Pienaar et al. 2011). When two sulcal graphs had different number of nodes, our method allowed their partial matches and decreased their similarity using a weighted penalty term based on the number of unmatched nodes ($w_{nc}nc$).

Furthermore, this method also allows variable weighting of geometric and topological features, to assess their relative importance on sulcal pattern similarity. First, all five features were optimally weighted in the sulcal pattern matching and similarity measure. Once given the optimal match between the nodes in different sulcal graphs, various similarities were measured by changing the weights. We evaluated the impact of each individual feature on similarity measures by setting all weights of the other features to 0. All sets of weights for the similarity measure are shown in Table 2. The set of all 5 weights ($w_{x,y,z} = 0.025$, $w_d = 0.8$, $w_s = 0.03$, $w_c = 0.1$, and $w_{nc} = 0.3$) were chosen through many experiments of matching between different brains in our previous study (Im, Pienaar et al. 2011). When we used only one non-zero weight, we simply multiplied the weight by 2 or 3 for an appropriate range of the similarity value. Figure 2 shows the example of the identification of sulcal pits and sulcal basins, and the construction of sulcal graphs and their optimal matching and similarity measure in the temporal lobe from two different brains. The sulcal basins paired by matching are marked with the same color and unmatched sulcal pits are colored black. We have previously explained the methodological procedures in more detail and showed that our algorithm extracted reliable similarity measures between sulcal graphs of different individual brains in spite of a large number of noisy sulcal pits and spatial deformations (Im, Pienaar et al. 2011).

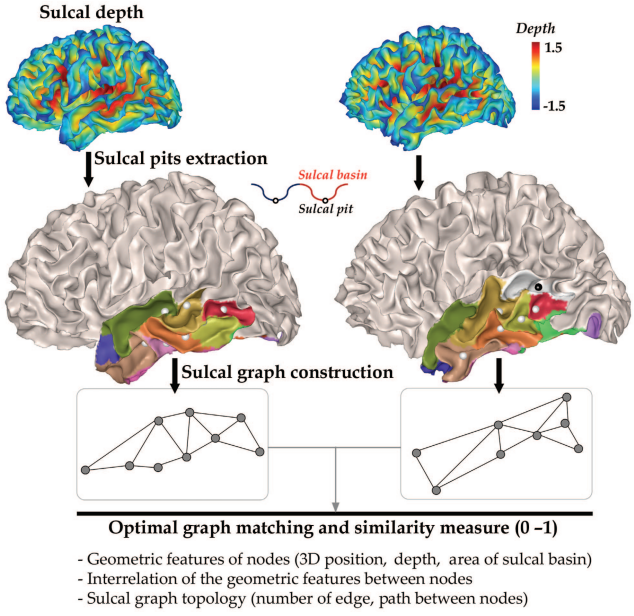

Figure 2. Similarity measure of the sulcal pattern in the temporal lobe between two different brains. Sulcal pits and their sulcal catchment basins are identified on the white matter surface using the watershed segmentation applied to sulcal depth map. Each sulcal pit corresponds to a node in the graph structure. When sulcal basins meet, sulcal pits in those basins are connected with an undirected edge. Two sulcal graphs are optimally matched and their similarity is measured by using the geometric features of nodes (3D position, depth and area of sulcal basin) and their relationship, and the graph topological features (the number of edges and the paths between nodes) and the number of unmatched nodes. The sulcal basins paired by matching are marked with the same color and unmatched sulcal pits are colored black.

Analysis of Sulcal Pattern Similarity with the Typical in PMG

Using our methodology, sulcal pattern similarities of all possible pairs were automatically computed and a similarity matrix (44×44) was constructed for left and right hemispheres and lobes with various sets of weights. We first tested whether the similarity within typical group was significantly different when compared with the similarity between typical and PMG groups. Each typical subject (a_i) had a mean similarity (S') with the other 25 typical subjects. For each PMG

Table 2
Sets of weights for sulcal pattern similarity measure

Weights				
$w_{x,y,z}$	w_d	w_s	w_c	w_{nc}
0.025	0.8	0.03	0.1	0.3
0.050	0	0	0	0
0	1.6	0	0	0
0	0	0.09	0	0
0	0	0	0.3	0
0	0	0	0	0.9

All five features are weighted in the sulcal pattern matching and similarity measure. In addition, only one feature is weighted and the other features are set to 0 to examine the effect of each individual feature on the sulcal pattern similarity.
$w_{x,y,z}$, w_d, w_s, w_c, and w_{nc} are weights for 3D position, sulcal depth, area of sulcal basin, graph topology, and the number of unmatched nodes between graphs, respectively.

subject (b_i), the mean similarity with all 26 typical subjects was calculated.

$$A = \{1, 2, 3, \ldots, 26\}, \quad B = \{1, 2, 3, \ldots, 18\}$$

$$S'(a_i) = \frac{\sum_{j \in A, i \neq j} S(a_i, a_j)}{n(A) - 1} \; (i \in A), \; S'(b_i) = \frac{\sum_{j \in A} S(b_i, a_j)}{n(A)} \; (i \in B),$$

where A and B are subject ID for typical and PMG groups, respectively, n is the number of subjects in the group, and S is the sulcal pattern similarity between two subjects. The differences between the typical and PMG in the mean similarity (S' (a) vs. S' (b)) were examined with an independent two sample t-test.

There were more females than males in the typical group and the reverse in the PMG group, accordingly gender ratio was a possible confounding effect on our analysis. Hence we checked whether the similarity between males and females was significantly lower than the similarity within the same gender in each group using the same approach described above. Moreover, we statistically compared the number of sulcal pits between the typical and PMG using the two sample t-test to examine whether the differences in the sulcal pattern were simply caused by the different number of pits.

To find the relationship between the similarity with the typical and the language function in the PMG, we compared the three PMG groups, which were divided according to the language score ranging from 1 to 3 (1: intact, 2: mild-to-moderate impairment, 3: profound impairment). We analyzed the mean similarities with typical subjects between the groups with the Kruskal–Wallis test, which is a nonparametric method for one-way analysis of variance. Since the difference among the three groups could occur by chance, a permutation-based test was carried out to correct for the occurrence of false positives. Data were randomly assigned to three groups at 10 000 times and test statistics were calculated for each data set. We counted the number of times the statistical value in the original data set was smaller than the statistical value obtained from the randomly resampled data sets, and divided that value by the number of random permutations (10 000). All statistical tests were performed for left and right hemispheres and lobes with several different sets of weights.

Quantitative Individual Analysis and Discrimination

We also examined whether the similarity of each individual PMG patient with the control group is outside the normal range by measuring its relative position in the distribution of all the typical controls. For example, see Figure 3 which shows a histogram of the distribution of similarity scores for the typical group, ranging from about 0.733 to about 0.763. For a given individual PMG patient b_i with score S' (b_i), we simply count the number of typical subjects that had a lower score, n' (b_i), and express that value as a ratio $R(b_i)$ to the total number of typical subjects ($n(A) = 26$). Thus, in the figure, S' (b_i) = 0.735, and only a single typical subject had a lower similarity value, resulting in a ratio $R(b_i)$ of 1/26. More formally,

$$R(b_i) = \frac{n'(b_i)}{n(A)}, \quad n'(b_i) = n\{a_j | S'(a_j) < S'(b_i)\} \quad (i \in B, j \in A).$$

In effect, $R(b_i)$ is the value of the cumulative distribution of the normal similarities at the similarity of a PMG subject b_i. This ratio ranges from 0 to 1 with the lower values indicating lower similarity between subject b_i and the space of all the typical controls. The PMG patients were visually inspected for lobar involvement, with a value of "1" in a lobe indicating involvement and a value of "0" indicating no involvement. In our quantitative analysis, if a patient had an $R(b_i)$ of less than 0.05 (= 5%) for some similarity measure S' (b_i) in a given lobe, that lobe was tagged as presenting an abnormal sulcal pattern. We then generated cross tables for each lobe comparing number of patients with obvious visual presentation of PMG to the frequency of values that were quantitatively measured with $R < 0.05$. A subsequent set of tables were also generated for cases, where $R = 0$.

The similarity values in the control group might not be accurately sampled such as in the tail of the distribution because it was not based on a large sample. Hence, we additionally performed a parametric modeling of the typical group distribution and statistical test as well as measuring the R value for the individual analysis. The individual similarity value of PMG patient S' (b_i) was compared with the similarity values of the typical controls S' (a) using a one sample t-test for all lobar regions. When a patient showed a significantly lower similarity than the typical group, that patient was discriminated as having abnormal sulcal pattern in a given lobe. For strict individual discrimination, the significance level was conservatively set to a threshold of $P = 10^{-5}$. The cross tables comparing the results of quantitative discrimination to visual diagnosis were also generated.

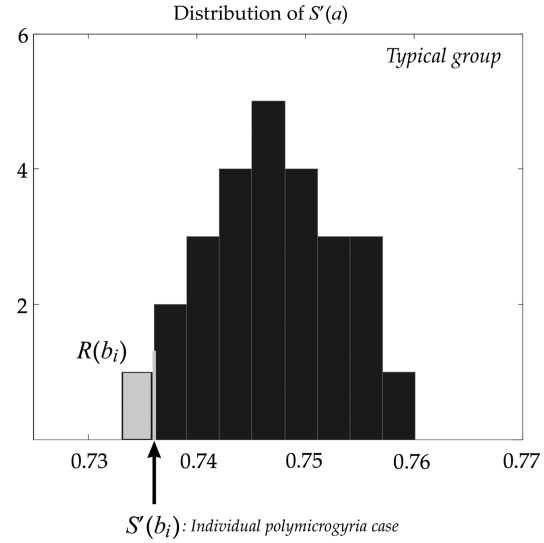

Figure 3. An example diagram for the definition of the ratio, R. S' (a) is the mean similarity of sulcal patterns which is measured for each typical subject with the other typical subjects, ranging from about 0.733 to about 0.763. S' (b_i) is the mean similarity value 0.735 between a PMG subject and all typical subjects. We count the number of the typical subjects that had a lower score, and express that value as a ratio $R(b_i)$ to the total number of typical subjects (= 26). In the figure, only a single typical subject had a lower similarity value, resulting in a ratio of 1/26.

		Visual diagnosis (per lobe)	
		Presenting with PMG	No PMG seen
Quantitative discrimination	Abnormal ($R < 0.05$ or $R = 0$, $P < 10^{-5}$)	a (number of patients)	b
	Typical ($R \geq 0.05$ or $R > 0$, $P \geq 10^{-5}$)	c	d

Cortical Mean Curvature Analysis

We measured the mean curvature on a discrete surface model of the inner cortex to characterize abnormal cortical folding in PMG brains (Pienaar et al. 2008). The original cortical surfaces had noisy features and small geometric variations in shape, and therefore their curvature maps were not smooth. We smoothed the curvature maps using a surface-based heat kernel smoothing with a full-width half-maximum value of 20 mm (Chung et al. 2005). The absolute values of the mean curvatures were measured to quantify the complexity of the cortical folding shape (Luders et al. 2006; Im, Lee, Lyttelton et al. 2008; Im, Choi et al. 2011) and averaged for left and right hemispheres and lobes. A previous study showed a significant relationship between the absolute mean curvature and the brain size measured by intracranial volume (Im, Lee, Lyttelton et al. 2008). The intracranial volumes were calculated after skull stripping (Dale et al. 1999) and the absolute mean curvatures were corrected for those volumes using linear

regression and obtaining residuals. We then performed the group analysis and individual discrimination using the same tests as explained above.

Results

Low Mean Similarity Between PMG and Typical Groups in the Sulcal Pattern

We first confirmed that there was no significant gender effect on our results. The similarity between males and females was not significantly different when compared with the similarity within the same gender in both typical and PMG groups for all regions. The PMG subjects showed a low mean similarity with the typical subjects in the sulcal pattern. Statistical tests were performed for each hemisphere and lobe with six sets of weights. For global analysis in the left and right hemispheres, the similarities between typical and PMG groups were significantly lower than the similarities measured within the typical group at the 0.05 level of P in all sets of features. The differences were highly significant at the 0.001 level of P for the whole feature, sulcal graph topology and the number of unmatched nodes in both hemispheres, and depth and area of sulcal basin in the left hemisphere. In the lobar regional sulcal pattern analysis using the whole feature, the mean similarities were significantly lower in the PMG than in the typical for all lobes ($P < 0.05$) except for the right occipital lobe. Among them, left temporal and parietal, and right frontal and parietal lobes showed strong statistical significances ($P < 0.001$). When using each feature independently, significantly lower mean similarities with the typical group were frequently observed in the PMG. However, the differences between the typical and PMG in the mean similarity were relatively low in both occipital lobes and right temporal lobe when compared with other regions. All statistical results are presented in Table 3. In the case of the number of sulcal pits, there was no significant difference between the two groups in all regions (Table S1 in Supplementary Material).

We found statistically significant relationship between abnormality of sulcal pattern and language function in PMG subjects. The group with intact language function showed significantly higher similarity with the typical than the impaired group in the depth (permutation test; $P = 0.019$) and the area of sulcal basin ($P = 0.009$) in the left parietal lobe. For these significant results, the distributions of the mean similarity with the typical group and the differences according to the language score are shown in box plots (Fig. 4). All statistical results for the comparison of the three PMG groups are provided in Supplementary Material Table S2.

Comparison Between Quantitative Discrimination and Visual Diagnosis

For example, Figure 5 shows visual diagnosis and the result of the quantitative ratios (R values) for the left hemisphere of the individual PMG. MRI volume image of the same brain is shown in Figure 1. For this patient, the frontal, temporal, and parietal lobes were diagnosed to have PMG pattern (= 1). Our quantitative ratios were also quite low in these lobes for a set of all features, which were under 0.05. Even the frontal and parietal lobes showed the 0 ratio, which means complete deviation from the distribution of normal sulcal patterns.

Table 3
Statistical results for the comparison of the similarity within typical group and the similarity between typical and PMG groups with different feature sets

	Hemisphere			Frontal			Temporal			Parietal			Occipital		
Feature	Typical	PMG	*P*-value	Typical	PMG	*P*-value	Typical	PMG	*P*-value	Typical	PMG	*P*-value	Typical	PMG	*P*-value
Left															
Total	0.727 (0.006)	0.705 (0.020)	<0.0001**	0.731 (0.008)	0.713 (0.026)	0.0014*	0.733 (0.015)	0.708 (0.024)	0.0001**	0.700 (0.014)	0.676 (0.027)	0.0006**	0.718 (0.015)	0.693 (0.035)	0.0027*
x, y, z	0.749 (0.009)	0.736 (0.016)	0.0014*	0.750 (0.008)	0.746 (0.011)	0.1320	0.753 (0.011)	0.730 (0.020)	<0.0001**	0.759 (0.011)	0.735 (0.022)	<0.0001**	0.735 (0.014)	0.727 (0.018)	0.0838
d	0.747 (0.006)	0.734 (0.015)	0.0003**	0.747 (0.008)	0.733 (0.015)	0.0004**	0.755 (0.017)	0.742 (0.023)	0.0321*	0.702 (0.013)	0.692 (0.024)	0.0607	0.726 (0.017)	0.720 (0.029)	0.3453
s	0.939 (0.004)	0.934 (0.004)	0.0002**	0.939 (0.005)	0.937 (0.006)	0.1019	0.931 (0.011)	0.925 (0.016)	0.1527	0.916 (0.008)	0.912 (0.009)	0.0961	0.931 (0.007)	0.926 (0.011)	0.0683
c	0.912 (0.004)	0.903 (0.008)	<0.0001**	0.925 (0.003)	0.920 (0.007)	0.0029*	0.935 (0.006)	0.929 (0.006)	0.0008**	0.932 (0.007)	0.928 (0.007)	0.0366*	0.916 (0.011)	0.908 (0.010)	0.0150*
nc	0.898 (0.009)	0.875 (0.027)	0.0003**	0.899 (0.015)	0.873 (0.054)	0.0230*	0.881 (0.046)	0.860 (0.062)	0.1947	0.855 (0.024)	0.833 (0.036)	0.0203*	0.906 (0.034)	0.870 (0.057)	0.0109*
Right															
Total	0.728 (0.008)	0.711 (0.013)	<0.0001**	0.734 (0.012)	0.719 (0.013)	0.0001**	0.733 (0.016)	0.718 (0.022)	0.0124*	0.708 (0.018)	0.675 (0.029)	<0.0001**	0.691 (0.032)	0.657 (0.082)	0.0615
x, y, z	0.750 (0.006)	0.740 (0.014)	0.0021*	0.753 (0.007)	0.745 (0.013)	0.0121*	0.745 (0.019)	0.732 (0.022)	0.0592	0.757 (0.011)	0.733 (0.026)	<0.0001**	0.731 (0.015)	0.732 (0.029)	0.9846
d	0.747 (0.009)	0.740 (0.015)	0.029*	0.746 (0.011)	0.740 (0.014)	0.0818	0.757 (0.018)	0.745 (0.023)	0.0679	0.718 (0.018)	0.699 (0.028)	0.0089*	0.705 (0.030)	0.702 (0.057)	0.8343
S	0.938 (0.004)	0.934 (0.007)	0.0136*	0.942 (0.006)	0.937 (0.007)	0.0245*	0.922 (0.011)	0.921 (0.010)	0.6117	0.920 (0.010)	0.905 (0.015)	0.0002**	0.931 (0.007)	0.927 (0.012)	0.1940
c	0.914 (0.005)	0.906 (0.008)	0.0002**	0.923 (0.003)	0.920 (0.005)	0.0150*	0.934 (0.006)	0.931 (0.009)	0.1537	0.936 (0.005)	0.927 (0.011)	0.0013*	0.906 (0.017)	0.894 (0.035)	0.1157
nc	0.898 (0.015)	0.878 (0.017)	0.0001**	0.907 (0.028)	0.884 (0.027)	0.0081*	0.893 (0.031)	0.882 (0.033)	0.2498	0.855 (0.026)	0.825 (0.051)	0.0155*	0.880 (0.049)	0.815 (0.113)	0.0129*

(*x*, *y*, *z*), *d*, *s*, *c*, and *nc* are features for 3D position, sulcal depth, area of sulcal basin, graph topology, and the number of unmatched nodes between graphs respectively.
Data: mean (standard deviation).
*$P < 0.05$.
**$P < 0.001$.

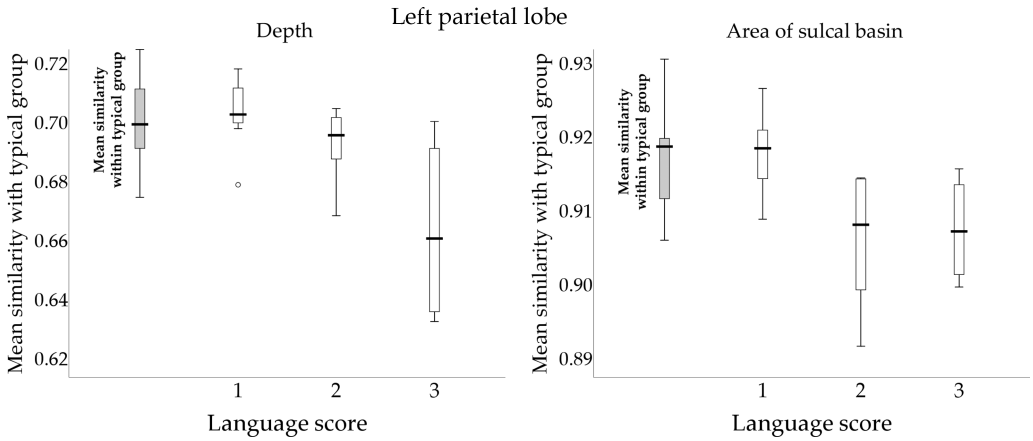

Figure 4. The box plots of the mean similarity with typical group in the depth and area of sulcal basin in the left parietal lobe for 3 PMG groups (1: intact, 2: mild-to-moderate impairment, 3: profound impairment). The group with unimpaired language function shows higher similarity with the typical than the impaired group.

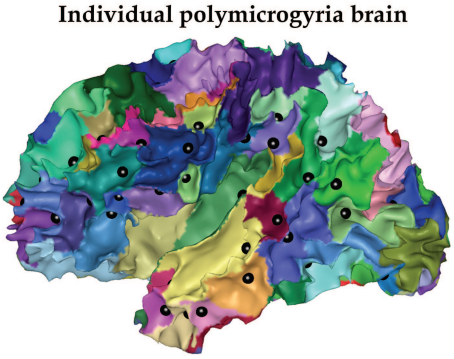

		Frontal	Temporal	Parietal	Occipital
Visual diagnosis		1	1	1	0
Quantitative ratio (*R*)	total	0.000**	0.038*	0.000**	0.423
	x, y, z	0.038*	0.115	0.000**	0.346
	d	0.000**	0.462	0.000**	0.346
	s	0.346	0.308	0.385	0.538
	c	0.000**	0.000**	0.154	0.154
	nc	0.000**	0.154	0.538	0.692

Figure 5. Visual diagnosis (1 = involved by PMG, 0 = notinvolved) and the quantitative ratio *R* for the left hemisphere of an individual PMG brain. Sulcal pits and their sulcal catchment basins are identified on the white matter surface. (*x ,y ,z*), *d*, *s*, *c*, and *nc* are features for 3D position, sulcal depth, area of sulcal basin, graph topology, and the number of unmatched nodes between graphs, respectively. MRI volume image of the same brain can be seen in Figure 1.

Table 4
Cross tables of quantitative discrimination and visual diagnosis

		Visual diagnosis					
Left	Frontal	PMG	No PMG	Temporal	PMG	No PMG
Quantitative discrimination ($R < 0.05$, $R = 0$; $P < 10^{-5}$)	Abnormal	11, 11 12	1, 1 3	Abnormal	9, 8 9	4, 4 7
	Typical	2, 2 1	4, 4 2	Typical	0, 1 0	5, 5 2
	Parietal	PMG	No PMG	Occipital	PMG	No PMG
	Abnormal	10, 8 10	2, 1 5	Abnormal	1, 0 0	11, 9 12
	Typical	0, 2, 0	6, 7 3	Typical	0, 1 1	6 / 8 5
Right						
	Frontal	PMG	No PMG	Temporal	PMG	No PMG
	Abnormal	9, 8 10	5, 5 6	Abnormal	6, 5 7	4, 1 5
	Typical	2, 3 1	2, 2 1	Typical	2, 3 1	6, 9 5
	Parietal	PMG	No PMG	Occipital	PMG	No PMG
	Abnormal	9, 8 9	4, 4 6	Abnormal	3, 2 3	4, 4 7
	Typical	0, 1 0	5, 5 3	Typical	0, 1 0	11, 11 8

Data: number of patients, first and second numbers in each cell are from the discrimination with the criteria of $R = 0.05$ and 0, respectively. Third numbers in the next line are the results with the *P*-value of 10^{-5}.

When observing the effect of each individual feature, one or more features showed the 0 ratio in each lobe.

The comparisons of quantitative discrimination with the ratio, $R < 0.05$ or $R = 0$, and visual diagnosis are shown in the cross tables for left and right four lobes with all patients (Table 4). When the abnormal pattern was indicated in some lobar regions by visual analysis, the quantitative method also found the abnormality in most cases (number of patients quantitatively detected as abnormal [$R < 0.05$]/visually diagnosed as PMG, left frontal: 11/13, left temporal: 9/9, left parietal: 10/10, left occipital: 1/1, right frontal: 9/11, right temporal: 6/8, right parietal: 9/9, right occipital: 3/3). Moreover, the quantitative discrimination determined more patients to be abnormal in all lobar regions than neuroradiologists visually diagnosed (number of patients detected quantitatively [$R < 0.05$] but not visually diagnosed, left frontal: 1, left temporal: 4, left parietal: 2, left occipital: 11, right frontal: 5, right temporal: 4, right parietal: 4, right occipital: 4). Only two cases were visually diagnosed but not detected quantitatively with the criteria of the 0.05 ratio in the left frontal and right frontal and temporal lobes.

Individual analysis based on a parametric statistical test also judged more lobar regions as abnormal than visual inspection detected for most patients (number of patients detected quantitatively [$P < 10^{-5}$] but not visually diagnosed, left frontal: 3, left temporal: 7, left parietal: 5, left occipital: 12, right frontal: 6, right temporal: 5, right parietal: 6, right occipital: 7) (Table 4). Abnormal sulcal patterns were not detected by the quantitative discrimination only for one patient in the left frontal and occipital and right frontal and temporal lobes.

Group and Individual Analyses of Absolute Mean Curvature

The absolute mean curvature in the PMG group was significantly higher than in the typical control group in the left frontal and parietal and right temporal lobes at the 0.05 level of *P*. In many patients with PMG diagnosed by visual inspection, the absolute mean curvature failed to detect a quantitative difference from typically developing brains. This was true for PMG visually diagnosed in all brain regions. In fact, using $R < 0.05$ for the quantitative threshold, only the following fraction of patients were classified as abnormal compared with the number visually diagnosed, left frontal: 6/13, left temporal: 1/9, left parietal: 5/10, left occipital: 0/1, right frontal: 2/11, right temporal: 1/8, right parietal: 1/9, right occipital: 0/3. A parametric statistical test also showed low sensitivity to detect the abnormal areas. Statistical results of the group difference and cross tables of quantitative discrimination and visual diagnosis are shown in Supplementary Material Tables S3 and S4.

Discussion

In this study, we provided quantitative measures detecting abnormal sulcal patterns in individual PMG brains using the methodology of graph-based sulcal pattern comparison and found their relationship with language function. We quantified a low similarity between typical and PMG sulcal patterns. These results were statistically significant using a group analysis. Although the significance level was different across different lobar regions, the similarities between typical and PMG groups were significantly lower than the similarities measured within the typical group at the 0.05 level of *P* for all lobes in one or more feature set. Additionally, for each individual PMG brain, we provided quantitative ratios indicating how similar its sulcal pattern was to the distribution of the typical sulcal patterns in each lobe with various feature sets. Our results showed quantifiable variable lobar involvement across different patients, which reconfirmed previous qualitative visual reports of the heterogeneous topographic distribution of PMG involvement (Barkovich et al. 2005; Leventer et al. 2010). To understand how genetic disorders can selective affect separate regions in the brain, it has been suggested that the proliferative zone during embryonic development consists of a heterogeneous population of progenitor cells that form a "protomap" and different cells or regions in this zone become separate targets for mutations in specific genes (Rakic 1988, 2004; Cholfin and Rubenstein 2008; Rakic 2009). This might cause region-specific and heterogeneous involvement of PMG across individuals. Development of a quantifiable measure to characterize regional involvement in individuals offers the potential to further explore potential genetic associations.

Our quantitative analysis using the sulcal pattern similarity showed high sensitivity to detect group differences and discriminate the abnormal areas that were visually detected. Furthermore, more lobar regions were determined to be abnormal in the quantitative discrimination in most patients when compared with the visual diagnosis even with the criteria of the 0 ratio or the low significance level. A common shape feature, mean curvature, was also used for the same group and individual analyses, but it was much less sensitive than the sulcal pattern similarity in detecting abnormal cortical areas. We demonstrated that the low sulcal pattern similarity with the typical in PMG was not just affected by the number of sulcal pits. Therefore, these findings suggest that the geometric features and inter-relationships of the sulcal pits and the shape of sulcal graph structure are the important measure that characterizes abnormal cortical structure. Further studies are required to determine whether our approach provides additional insights into the genetic classification or clinical phenotype of PMG brains by providing quantitative imaging features that are difficult to detect by visual inspection alone.

The human brain develops the complex structural and functional connectivity networks, which have been increasingly elucidated by modern brain imaging techniques, such as diffusion tensor imaging (DTI) and functional MRI (Hagmann et al. 2011). Cortical areas do not develop independently, but develop in relation to other areas (Leingartner et al. 2007; O'Leary et al. 2007). This concept of interdependence of cortical regions during development supports our results that found more cortical involvement of PMG than visually perceived. We suggest that PMG may have a secondary more global effect on cortical folding, different from the frank high frequency gyration that is visually perceivable, that is below the threshold of visual detection. Thus, although some focal areas are malformed and visibly detected, other areas might be also affected and changed more subtly due to changes in brain connectivity. These structural changes deviated from the typical pattern would be compensatory or secondary to the primary involvement. Future studies will be aimed at analyzing the relationship between the sulcal patterns we detect and structural or functional connectivity.

Most malformations of cortical development do not involve the entire cortex equally. Typical imaging features show a region of maximal disruption of gyral folding and decreasing severity extending away from that region, that is, a severity gradient (Leventer et al. 2010). The severity gradient has been found to be important in genotype–phenotype correlation for some malformations of cortical development. For example, in the case of lissencephaly, an anterior > posterior severity gradient pattern was associated with mutations of the *DCX* gene and the posterior > anterior pattern was associated with mutations of the *LIS1* gene (Pilz et al. 1998; Dobyns et al. 1999). The severity gradient of PMG involvement has been visually investigated based on MR imaging patterns with the concept that it may correlate with the underlying molecular basis in PMG (Leventer et al. 2010). Our analysis shows that the severity gradient can be perceived in the individual table of the quantitative measurement, although we still need to define a more systematic way to determine the severity gradient. For example, an individual PMG brain in Figure 5 shows lower *R* ratios in more feature sets in the frontal lobe than other lobes. We can notice the approximate severity gradient from the maximal severity in the frontal lobe decreasing in the parietal and temporal regions. Therefore, our method could play an important role in providing an explicit unbiased imaging phenotype for investigating the pathogenesis of cortical malformations and genotype–phenotype correlation.

Our ability to show significant differences in left parietal sulcal patterns in subjects with language impairment is consistent with a previous study of language disorders in PMG (Guerreiro et al. 2002). Severe clinical manifestation of developmental language disorder was present when the PMG

pattern occurred around the entire extent of the sylvian fissure, including the parietal region. The patients with PMG restricted to the posterior parietal regions also had a mild form of developmental language disorder (Guerreiro et al. 2002). Another recent DTI study found that the arcuate fasciculus could not be identified by fiber tracking in PMG patients with severe impairment and no speech development (Saporta et al. 2011). The left arcuate fasciculus is involved in language function as it connects the perisylvian cortex including the parietal lobe (Catani and Thiebaut de Schotten 2008). Consequently our results in the left parietal lobe could be related to changes of axonal pathways involved in language function. Limitation of this analysis was the lack of multiple assessment of language function. Future studies will further investigate quantitative correlations between more clinical and imaging features including DTI.

Our automatic detection of abnormal sulcal patterns was not successful for all PMG patients. Abnormal patterns in some lobar regions of PMG were not detected by the quantitative method in a small number of patients with the 0.05 ratio (two patients in the left frontal and right frontal and temporal lobes). We reviewed the raw images of those patients to investigate the characteristics of the visually perceived PMG regions. In these cases, the extent of PMG was localized to a small region of the lobe and the cortical surface model exhibited abnormal shape in the region of the high frequency gyration. However, when confined to such a small area, the quantitative analysis was dominated by the neighboring gyral structure and hence the global folding pattern was not affected. Thus our method shows a limitation in detecting small, localized abnormalities. In future work, we will explore the ability of local shape information to improve the detection of localized PMG and believe the addition of local shape information will provide a more complete description of gyral folding.

This study was based on a small set of patients, 18 PMG patients. The ages of the patients were variable and their distribution was wide, ranging from 2 to 18 years. We carefully matched the age distribution and composed the control group with 26 typical developing subjects. Group analysis or individual patient discrimination with a different control set using a larger number of subjects may be useful to reduce false positives. However, to date, this is the largest PMG population studied with quantitative analysis as previous quantitative imaging studies were primarily case studies based on a small number of patients due to limitation of image acquisition for patients and the lack of the use of advanced image analysis techniques (Munakata et al. 2006; Trivedi et al. 2006; Oliveira et al. 2009; Saporta et al. 2011). Our study is based on the new automated method for quantitative image analysis with a relatively larger set of patients when compared with these prior studies. For data analysis, several approaches were employed to acquire robust results with our data set. Since the three subgroups of PMG patients determined by the language score were small, a permutation-based non-parametric test was carried out for reliable statistical group analysis. In the individual analysis and patient discrimination, we performed a parametric statistical test as well as histogram ranking from the distribution of the typical controls. The parametric statistical test showed that significantly abnormal sulcal patterns were detected in most patients even at the extremely low significance threshold of P-value ($<10^{-5}$) (Table 4). Thus, although, patients numbers are small, this is the largest report to date and we believe we have adequately controlled for false positives and have demonstrated the potential of our approach.

In conclusion, our sulcal pattern analysis showed potential for providing a quantitative and reliable means for measuring the severity and extent of cortical involvement in PMG in relation to clinical and functional deficits. This method might be helpful in detecting and investigating the significance of additional cortical folding abnormalities not visually detected and may provide a more rigorous means to explore genotype–phenotype correlations and clinical phenotype-imaging correlations.

Supplementary Material

Supplementary material can be found at: http://www.cercor.oxfordjournals.org/.

Funding

This work was supported by the Foundation of the American Society of Neuroradiology, Scholar Award in Neuroradiology Research 2011.

Notes

Conflict of Interest: None declared.

References

Barkovich AJ. 2010. MRI analysis of sulcation morphology in polymicrogyria. Epilepsia. 51(Suppl 1):17–22.

Barkovich AJ, Kjos BO. 1992. Nonlissencephalic cortical dysplasias: correlation of imaging findings with clinical deficits. AJNR Am J Neuroradiol. 13:95–103.

Barkovich AJ, Kuzniecky RI, Jackson GD, Guerrini R, Dobyns WB. 2005. A developmental and genetic classification for malformations of cortical development. Neurology. 65:1873–1887.

Catani M, Thiebaut de Schotten M. 2008. A diffusion tensor imaging tractography atlas for virtual in vivo dissections. Cortex. 44:1105–1132.

Chang BS, Apse KA, Caraballo R, Cross JH, McLellan A, Jacobson RD, Valente KD, Barkovich AJ, Walsh CA. 2006. A familial syndrome of unilateral polymicrogyria affecting the right hemisphere. Neurology. 66:133–135.

Chang BS, Piao X, Bodell A, Basel-Vanagaite L, Straussberg R, Dobyns WB, Qasrawi B, Winter RM, Innes AM, Voit T *et al.* 2003. Bilateral frontoparietal polymicrogyria: clinical and radiological features in 10 families with linkage to chromosome 16. Ann Neurol. 53:596–606.

Chang BS, Piao X, Giannini C, Cascino GD, Scheffer I, Woods CG, Topcu M, Tezcan K, Bodell A, Leventer RJ *et al.* 2004. Bilateral generalized polymicrogyria (BGP): a distinct syndrome of cortical malformation. Neurology. 62:1722–1728.

Cholfin JA, Rubenstein JL. 2008. Frontal cortex subdivision patterning is coordinately regulated by Fgf8, Fgf17, and Emx2. J Comp Neurol. 509:144–155.

Chung MK, Robbins SM, Dalton KM, Davidson RJ, Alexander AL, Evans AC. 2005. Cortical thickness analysis in autism with heat kernel smoothing. Neuroimage. 25:1256–1265.

Dale AM, Fischl B, Sereno MI. 1999. Cortical surface-based analysis. I. Segmentation and surface reconstruction. Neuroimage. 9:179–194.

Desikan RS, Segonne F, Fischl B, Quinn BT, Dickerson BC, Blacker D, Buckner RL, Dale AM, Maguire RP, Hyman BT *et al.* 2006. An automated labeling system for subdividing the human cerebral

cortex on MRI scans into gyral based regions of interest. Neuroimage. 31:968–980.
Dobyns WB, Truwit CL, Ross ME, Matsumoto N, Pilz DT, Ledbetter DH, Gleeson JG, Walsh CA, Barkovich AJ. 1999. Differences in the gyral pattern distinguish chromosome 17-linked and X-linked lissencephaly. Neurology. 53:270–277.
Fischl B, Liu A, Dale AM. 2001. Automated manifold surgery: constructing geometrically accurate and topologically correct models of the human cerebral cortex. IEEE Trans Med Imaging. 20:70–80.
Fischl B, Sereno MI, Dale AM. 1999. Cortical surface-based analysis. II: inflation, flattening, and a surface-based coordinate system. Neuroimage. 9:195–207.
Fischl B, van der Kouwe A, Destrieux C, Halgren E, Segonne F, Salat DH, Busa E, Seidman LJ, Goldstein J, Kennedy D *et al.* 2004. Automatically parcellating the human cerebral cortex. Cereb Cortex. 14:11–22.
Gaser C, Luders E, Thompson PM, Lee AD, Dutton RA, Geaga JA, Hayashi KM, Bellugi U, Galaburda AM, Korenberg JR *et al.* 2006. Increased local gyrification mapped in Williams syndrome. Neuroimage. 33:46–54.
Guerreiro MM, Hage SR, Guimaraes CA, Abramides DV, Fernandes W, Pacheco PS, Piovesana AM, Montenegro MA, Cendes F. 2002. Developmental language disorder associated with polymicrogyria. Neurology. 59:245–250.
Guerrini R, Barkovich AJ, Sztriha L, Dobyns WB. 2000. Bilateral frontal polymicrogyria: a newly recognized brain malformation syndrome. Neurology. 54:909–913.
Guerrini R, Dubeau F, Dulac O, Barkovich AJ, Kuzniecky R, Fett C, Jones-Gotman M, Canapicchi R, Cross H, Fish D *et al.* 1997. Bilateral parasagittal parietooccipital polymicrogyria and epilepsy. Ann Neurol. 41:65–73.
Hagmann P, Sporns O, Madan N, Cammoun L, Pienaar R, Wedeen VJ, Meuli R, Thiran JP, Grant PE. 2011. White matter maturation reshapes structural connectivity in the late developing human brain. Proc Natl Acad Sci USA. 107:19067–19072.
Im K, Choi YY, Yang JJ, Lee KH, Kim SI, Grant PE, Lee JM. 2011. The relationship between the presence of sulcal pits and intelligence in human brains. Neuroimage. 55:1490–1496.
Im K, Jo HJ, Mangin JF, Evans AC, Kim SI, Lee JM. 2010. Spatial distribution of deep sulcal landmarks and hemispherical asymmetry on the cortical surface. Cereb Cortex. 20:602–611.
Im K, Lee JM, Lyttelton O, Kim SH, Evans AC, Kim SI. 2008. Brain size and cortical structure in the adult human brain. Cereb Cortex. 18:2181–2191.
Im K, Lee JM, Seo SW, Hyung Kim S, Kim SI, Na DL. 2008. Sulcal morphology changes and their relationship with cortical thickness and gyral white matter volume in mild cognitive impairment and Alzheimer's disease. Neuroimage. 43:103–113.
Im K, Pienaar R, Lee JM, Seong JK, Choi YY, Lee KH, Grant PE. 2011. Quantitative comparison and analysis of sulcal patterns using sulcal graph matching: a twin study. Neuroimage. 57:1077–1086.
Jansen A, Andermann E. 2005. Genetics of the polymicrogyria syndromes. J Med Genet. 42:369–378.
Kuzniecky R, Andermann F, Guerrini R. 1993. Congenital bilateral perisylvian syndrome: study of 31 patients. The CBPS Multicenter Collaborative Study. Lancet. 341:608–612.
Leingartner A, Thuret S, Kroll TT, Chou SJ, Leasure JL, Gage FH, O'Leary DD. 2007. Cortical area size dictates performance at modality-specific behaviors. Proc Natl Acad Sci USA. 104:4153–4158.
Leordeanu M, Hebert M. 2005. A spectral technique for correspondence problems using pairwise constraints. ICCV '05: Proceedings of the Tenth IEEE International Conference on Computer Vision IEEE Computer Society, Washington, DC, USA. 1482–1489.
Leventer RJ, Jansen A, Pilz DT, Stoodley N, Marini C, Dubeau F, Malone J, Mitchell LA, Mandelstam S, Scheffer IE *et al.* 2010. Clinical and imaging heterogeneity of polymicrogyria: a study of 328 patients. Brain. 133:1415–1427.
Lohmann G, von Cramon DY, Colchester AC. 2008. Deep sulcal landmarks provide an organizing framework for human cortical folding. Cereb Cortex. 18:1415–1420.
Luders E, Thompson PM, Narr KL, Toga AW, Jancke L, Gaser C. 2006. A curvature-based approach to estimate local gyrification on the cortical surface. Neuroimage. 29:1224–1230.
Lyu I, Seong JK, Shin SY, Im K, Roh JH, Kim MJ, Kim GH, Kim JH, Evans AC, Na DL *et al.* 2010. Spectral-based automatic labeling and refining of human cortical sulcal curves using expert-provided examples. Neuroimage. 52:142–157.
Mangin JF, Jouvent E, Cachia A. 2010. In vivo measurement of cortical morphology: means and meanings. Curr Opin Neurol. 23:359–367.
Munakata M, Onuma A, Takeo K, Oishi T, Haginoya K, Iinuma K. 2006. Morphofunctional organization in three patients with unilateral polymicrogyria: combined use of diffusion tensor imaging and functional magnetic resonance imaging. Brain Dev. 28:405–409.
O'Leary DD, Chou SJ, Sahara S. 2007. Area patterning of the mammalian cortex. Neuron. 56:252–269.
Oliveira PP Jr, Valente KD, Shergill SS, Leite Cda C, Amaro E Jr. 2009. Cortical thickness reduction of normal appearing cortex in patients with polymicrogyria. J Neuroimaging. 20:46–52.
Piao X, Basel-Vanagaite L, Straussberg R, Grant PE, Pugh EW, Doheny K, Doan B, Hong SE, Shugart YY, Walsh CA. 2002. An autosomal recessive form of bilateral frontoparietal polymicrogyria maps to chromosome 16q12.2-21. Am J Hum Genet. 70:1028–1033.
Piao X, Hill RS, Bodell A, Chang BS, Basel-Vanagaite L, Straussberg R, Dobyns WB, Qasrawi B, Winter RM, Innes AM *et al.* 2004. G protein-coupled receptor-dependent development of human frontal cortex. Science. 303:2033–2036.
Pienaar R, Fischl B, Caviness V, Makris N, Grant PE. 2008. A methodology for analyzing curvature in the developing brain from preterm to adult. Int J Imaging Syst Technol. 18:42–68.
Pilz DT, Matsumoto N, Minnerath S, Mills P, Gleeson JG, Allen KM, Walsh CA, Barkovich AJ, Dobyns WB, Ledbetter DH *et al.* 1998. LIS1 and XLIS (DCX) mutations cause most classical lissencephaly, but different patterns of malformation. Hum Mol Genet. 7:2029–2037.
Rakic P. 2009. Evolution of the neocortex: a perspective from developmental biology. Nat Rev Neurosci. 10:724–735.
Rakic P. 2004. Neuroscience. Genetic control of cortical convolutions. Science. 303:1983–1984.
Rakic P. 1988. Specification of cerebral cortical areas. Science. 241:170–176.
Regis J, Mangin JF, Ochiai T, Frouin V, Riviere D, Cachia A, Tamura M, Samson Y. 2005. "Sulcal root" generic model: a hypothesis to overcome the variability of the human cortex folding patterns. Neurol Med Chir (Tokyo). 45:1–17.
Rettmann ME, Kraut MA, Prince JL, Resnick SM. 2006. Cross-sectional and longitudinal analyses of anatomical sulcal changes associated with aging. Cereb Cortex. 16:1584–1594.
Saporta AS, Kumar A, Govindan RM, Sundaram SK, Chugani HT. 2011. Arcuate fasciculus and speech in congenital bilateral perisylvian syndrome. Pediatr Neurol. 44:270–274.
Segonne F, Dale AM, Busa E, Glessner M, Salat D, Hahn HK, Fischl B. 2004. A hybrid approach to the skull stripping problem in MRI. Neuroimage. 22:1060–1075.
Segonne F, Pacheco J, Fischl B. 2007. Geometrically accurate topology-correction of cortical surfaces using nonseparating loops. IEEE Trans Med Imaging. 26:518–529.
Sled JG, Zijdenbos AP, Evans AC. 1998. A nonparametric method for automatic correction of intensity nonuniformity in MRI data. IEEE Trans Med Imaging. 17:87–97.
Trivedi R, Gupta RK, Hasan KM, Hou P, Prasad KN, Narayana PA. 2006. Diffusion tensor imaging in polymicrogyria: a report of three cases. Neuroradiology. 48:422–427.